Full Title: Large-scale neuroimaging and genetic study reveals genetic architecture of brain white matter microstructure

Running Title: Genetic architecture of brain white matter

Bingxin Zhao, M.S.[1], Jingwen Zhang, B.S.[1], Joseph G. Ibrahim, Ph.D.[1], Rebecca C. Santelli, Ph.D.[2], Yun Li, Ph.D.[1,3,4], Tengfei Li, Ph.D.[5], Yue Shan, B.S.[1], Ziliang Zhu, B.S.[1], Fan Zhou, M.S.[1], Huiling Liao. B.S.[6], Thomas E. Nichols, Ph.D.[7,8], and Hongtu Zhu, Ph.D.*[1,5]

[1] Departments of Biostatistics, [2] Psychiatry, [3] Genetics, and [4] Computer Science, University of North Carolina at Chapel Hill, Chapel Hill, NC, USA, 27599

[5] Department of Biostatistics, The University of Texas MD Anderson Cancer Center, Houston, TX, USA, 77230

[6] Department of Statistics, Texas A&M University, College Station, TX, USA, 77843

[7] Wellcome Trust Centre for Integrative Neuroimaging, Big Data Institute, University of Oxford, Oxford, UK, OX1 2JD

[8] Department of Statistics, University of Warwick, Coventry, UK, CV4 7AL

**Corresponding author*:

Hongtu Zhu

Department of Biostatistics, University of North Carolina at Chapel Hill,

3105C McGavran-Greenberg Hall, Chapel Hill, NC 27599.

Email address: htzhu@email.unc.edu Phone: (919) 966-7250

Abstract

Microstructural changes of white matter (WM) tracts are known to be associated with various neuropsychiatric disorders. We comprehensively analyzed the genetic architecture of WM tracts using diffusion tensor imaging (DTI) and genome-wide single-nucleotide polymorphism (SNP) data. We created the tract-based (p = 441) and voxel-wise DTI parameters using the ENIGMA-DTI pipeline. The genetic architecture was estimated in univariate or bivariate linear mixed-effects models (n ~ 8000), and polygenic risk scores were employed to detect the significant genetic overlap between WM tracts and four neuropsychiatric disorders. We found the DTI parameters are substantially heritable for most WM tracts (mean heritability 48.6%). Enrichment of genetic effects was observed for SNPs that are active in central nervous system (CNS) cells (p-value < $2.2*10^{-16}$). Significant genetic overlap was detected for attention-deficit /hyperactivity disorder (ADHD) and internal capsule (p-value < 0.0025), and for autism spectrum disorder (ASD) and cingulum cingulate gyrus as well as corpus callosum (p-value < 0.0029). Voxel-level analysis displayed the heterogeneity of vertex-wise heritability within the WM tracts, and bivariate analysis illustrated the genetic

connections among WM tracts as well as DTI parameters. These results suggested that the DTI parameters are heritable and are likely to have shared genetic basis with neuropsychiatric traits.

Key Words: DTI, neuropsychiatric traits, polygenic risk scores, SNP heritability, white matter microstructure.

Introduction

Complex brain functions rely on dynamic interactions between distributed brain areas operating in large-scale networks. Consequently, the integrity of white matter connections between brain areas is critical to proper function. Microstructural differences in white matter (WM) tracts are associated with information processing speed and intelligence (Penke L et al. 2010; Tamnes CK et al. 2010; Penke L et al. 2012; Ritchie SJ, ME Bastin, et al. 2015; Ritchie SJ, T Booth, et al. 2015) as well as neuropsychiatric traits, such as Alzheimer's disease (Nir TM et al. 2013), Schizophrenia (SCZ) (Voineskos AN 2015), attention-deficit/hyperactivity disorder (ADHD) (Sudre G et al. 2017) and anorexia nervosa (Vogel K et al. 2016). A better understanding of genetic factors influencing integrity of WM tracts could have important implication for understanding the etiology of these diseases as well as individual variation in intelligence. To reveal the underlying genetic contributions to brain structural development and disease/disorder processes, imaging genetics studies of WM microstructure has been an active research area over the past fifteen years. The structural changes of WM tracts are typically measured and quantified in diffusion

tensor imaging (Basser PJ et al. 1994) (DTI). Brain diffusivity can be influenced by many aspects of its micro- or macro-structures (Beaulieu C 2002). To reconstruct the WM pathways and tissue microstructure, DTI models the diffusion properties of WM using random movement of water. Specifically, DTI quantifies diffusion magnetic resonance imaging (dMRI) in a tensor model and analyze diffusions in all directions. A typical DTI diagonalizes the tensor and calculates three pairs of eigenvalues/eigenvectors that respectively represent one primary and two secondary diffusion directions. Within each voxel, several DTI parameters can be derived: fractional anisotropy (FA), mean diffusivity (MD), axial diffusivity (AD), radial diffusivity (RD), and mode of anisotropy (MO). As a summary measure of WM integrity (Thomason ME and PM Thompson 2011; Jones DK et al. 2013), higher FA indicates stronger directionality in this voxel. MD quantifies the magnitude of absolute directionality, AD is the eigenvalue of the principal direction, RD is the average of the eigenvalues of the two secondary directions, and MO is the third moment of a tensor. Positive MO reflects narrow tubular water diffusion, whereas a negative value denotes planar water diffusion (Cox SR et al. 2016). There are several approaches to analyze DTI data across the whole brain, including manual

region-of-interest (ROI) analysis, automated ROI analysis, voxel-based analysis, such as tract-based spatial statistics (Smith SM et al. 2006) (TBSS), as well as tractography and graph theory analysis; see Tamnes CK et al. (2017) for a survey.

In family-based studies, the magnitude of genetic influences (i.e., heritability) in various DTI parameters of WM tracts, including FA, MD, AD, and RD, has been examined across a wide age range, from neonates (Geng X et al. 2012; Lee SJ et al. 2015), young children (Lee SJ et al. 2017), older children (Brouwer RM et al. 2010; Brouwer RM et al. 2012), adolescents (Chiang M-C et al. 2011), and young adults (Kochunov P et al. 2015) to middle aged (Vuoksimaa E et al. 2017) and older adults (Kanchibhotla SC et al. 2013). Participants in these studies are typically monozygotic and dizygotic twins or family members. Table 1 of Vuoksimaa E *et al.* (2017) lists 14 studies that illustrated that a substantial proportion of variance in DTI parameters (FA, MD, AD, and RD) was explained by additive genetic effects. However, the genetic architecture of DTI parameters remains largely unknown due to the limitation of family-based studies, for which the heritability estimation has relied on contrasting the phenotypic similarity

between monozygotic and dizygotic twins. Genetic architecture denotes the characteristics of genetic variations that contribute to the broad-sense heritability of a phenotype (Timpson NJ et al. 2017). Uncovering the genetic architecture is an essential step to properly model the genetic influences on brain structures and neuropsychiatric traits. Based on the number of genetic variants contributing to phenotypic variance, genetic architecture can be described as monogenic (one variant), oligogenic (few variants), polygenic (many variants), or omnigenic, which hypothesizes that almost all genetic variants have small but non-zero genetic contributions (Badano JL and N Katsanis 2002; Boyle EA et al. 2017).

Recent developments have enabled heritability estimation and genetic architecture examination with using the common single-nucleotide polymorphisms (SNPs) data collected in general populations (Yang J, SH Lee, et al. 2011; Bulik-Sullivan BK et al. 2015; Loh P-R et al. 2015). Instead of using the expected genetic correlation based on pedigree information, SNP heritability is estimated by adding up the genetic effects across a large number of common SNPs (minor allele frequency [MAF] > 0.05 or 0.01). The

architecture of genetic influences can also be assessed by SNP annotation and partition (Yang J, TA Manolio, et al. 2011). With these methods, the availability of genomic and imaging data from recent large population-based studies offers the opportunity to uncover the genetic basis of brain. Particularly, the United Kingdom (UK) Biobank resource (Sudlow C et al. 2015) enables us to conduct SNP heritability analysis of brain WM tracts in one large-scale, relatively homogeneous population. The UK Biobank has captured data from over 500,000 original participants of middle or elderly ages (age range 40-69), and is currently in the process of following up with 100,000 of these participants to perform brain MRI screening. Imaging data of the first 10,000 subjects have recently been released for public research access (Alfaro-Almagro F et al. 2017).

Here, we used all common (MAF > 0.01) autosomal SNPs to analyze the genetic architecture of DTI parameters in 21 main WM tracts, as well as in 42 WM sub-tracts. In addition to FA, AD, RD, MD and MO, we examined the two secondary diffusion direction eigenvalues, respectively denoted as L2 and L3. The DTI data were generated using the ENIGMA-DTI pipeline (Thompson PM et al. 2014). We also refer to AD as L1, since AD is

essentially the eigenvalue of the primary diffusion direction. We partitioned genetic variation into individual chromosomes to examine the distribution of genetic effects across the genome. To assess the enrichment of SNPs in active chromatin regions, we partitioned genetic variation according to cell-type-specific functional annotations (Finucane HK et al. 2015). We further examined the genetic correlation for several pairs of DTI parameters and their relationship with the corresponding phenotypic correlation across WM tracts. We estimated gender-specific heritability for each DTI parameter in the main WM tracts and mapped the symmetric pattern of heritability in WM sub-tracts in the left and right hemispheres. We also performed voxel-level analysis to illustrate the heterogeneity of distribution of genetic effects on selected parts of the TBSS skeleton. Finally, to detect significant genetic overlap of WM tracts and neuropsychiatric traits, we created polygenic risk profiles in our UK Biobank samples using the published genome-wide association studies (GWAS) summary statistics from the Psychiatric Genomics Consortium (PGC, http://www.med.unc.edu/pgc) (Sklar P 2017; Sullivan PF et al. 2017).

Materials and Methods

Participants and image preprocessing

Datasets used in this paper are the UK Biobank, Philadelphia Neurodevelopmental Cohort (Satterthwaite TD et al. 2014) (PNC), and Pediatric Imaging, Neurocognition, and Genetics (Jernigan TL et al. 2016) (PING). Detailed data collection and processing procedures and quality control prior to the release of data are documented at http://www.ukbiobank.ac.uk/resources/ for the UK Biobank, http://pingstudy.ucsd.edu/resources/genomics-core.html for PING, and https://www.ncbi.nlm.nih.gov/projects/gap/cgi-bin/study.cgi?study_id=phs000607.v1.p1 for PNC. For each dataset, we used subjects with both DTI and SNP data available after applying consistent quality controls. To generate the DTI parameters, we ran the TBSS-ENIGMA pipeline (Thompson PM *et al.* 2014) with the FSL toolset (Jenkinson M et al. 2012). A full description of our DTI pipeline and quality control is documented in Supplementary Methods and an overview is given in Supplementary Figure 1. The demographic information for the DTI datasets is listed in Supplementary Table 1.

Genotyping

For the UK Biobank, we used their raw (non-imputed) genotype data released in July 2017. Genotype imputation was previously performed on the PNC and PING datasets. A full description of imputation procedures in the two datasets is provided in Supplementary Methods. Heritability estimates using imputed and non-imputed genotype data are usually similar (Davis LK et al. 2013). On each of the three SNP datasets, we used all autosomal SNPs and applied the same set of standard quality control procedures using the Plink toolset (Purcell S et al. 2007): excluding subjects with more than 10% missing genotypes, only including SNPs with MAF > 0.01, genotyping rate > 90%, and passing Hardy-Weinberg test (p-value > $1*10^{-7}$). We further removed any non-European subjects. To avoid including closely related relatives, we only used biologically unrelated subjects and excluded one of any pair of individuals with estimated genetic relationship larger than 0.025. The sample sizes of the datasets after conducting all quality control procedures are listed in Supplementary Table 2.

Statistical analysis

Global heritability

For each DTI parameter, we estimated the proportion of variation explained by autosomal SNPs with linear mixed-effects model (LMM) in each WM tract. There are 63 tracts (21 main tracts and 42 sub-tracts), each of them has seven DTI parameters. The formal setting of the LMM and definition of likelihood ratio test statistics can be found in Yang J et al. (2010) and we used the GCTA software (Yang J, SH Lee*, et al.* 2011) in our analyses. The basic idea is to fit the genetic relationship matrix (GRM) as a variance-covariance structure of random genetic effects, while adjusting for other covariates modelled with fixed effects. As mentioned before, we used 0.025 as the threshold in GRM to avoid including closely related relatives. Then the heritability of a phenotype is estimated by contrasting the genetic similarity among individuals with their phenotypic similarity in the LMM. We considered the fixed effects of age (at imaging visit), sex, and top ten genetic principal components. The same set of covariates are adjusted in all the heritability analysis below, unless stated otherwise. We corrected for multiple testing using the false discovery rate (FDR) method (Storey JD 2002) at 0.05 level.

Heritability explained by subset of SNPs

We re-estimated the GRMs using SNPs from each chromosome (22 GRMs in total) and used these GRMs separately to estimate the SNP heritability each at a time. We also put all the 22 GRMs into one model and estimate the SNP heritability simultaneously.

In addition, we partitioned the SNPs according to cell-type-specific annotations (36, 45) to perform enrichment analysis. SNPs are grouped according to their general functional activeness in various cell groups. In DTI analysis, we particularly focused on the activeness in the central nervous system (CNS) cell group, and thus we clustered all SNPs into three main categories: CNS_active (n = 98,889), CNS_inactive (n = 148,282), and Always_inactive (n = 205,742), see Supplementary Methods for detailed definitions. We estimated the SNP heritability explained by these GRMs in one model.

Genetics correlations of WM tracts

In each tract, we performed bivariate genetic correlation analysis for the set of DTI parameters L1 (AD), L2, L3 and the set FA, RD, MD, MO on each of the main WM tracts.

In our analyses, GCTA software did not converge well for many DTI parameters. Thus, we switched to the BOLT-REML toolset (Loh P-R *et al.* 2015) to estimate the genetic correlation. The formal setting of the bivariate LMM and definition of genetic correlation can be found in Lee SH et al. (2012); Loh P-R *et al.* (2015). Similarly, we also performed pairwise genetic correlation analysis on the main WM tracts for each of the seven DTI parameters.

Polygenic Scoring

Polygenic profiles were created in the UK Biobank samples for several neuropsychiatric disorders: ADHD, autism spectrum disorder (ASD), bipolar disorder (BD), and Schizophrenia (SCZ). The published GWAS summary statistics were gathered from the PGC. Original studies can be found in Demontis D et al. (2017) for ADHD, Lee SH et al. (2013) for ASD, and Ruderfer DM et al. (2018) for BD and SCZ, where the participants are not overlapped with the UK Biobank individuals in this study. After linkage disequilibrium (LD) pruning with $R^2 = 0.2$ and window size 50, the remaining 230,072 SNPs are used to construct the scores. Since we found the DTI parameters have a highly

polygenic genetic architecture, we use all pruned SNPs to calculate the polygenic risk cores (Zhao B and F Zou 2018). Specifically, we used the Plink toolset (Purcell S *et al.* 2007) to generate one score separately for each disorder by summarizing across all the pruned SNP alleles, weighed by their effect sizes (log odds ratios). The association between each pair of polygenic profile and DTI parameter was estimated and tested in linear regression, adjusting for the same set of covariates as in heritability analysis. Again, we corrected for multiple testing by controlling FDR at 0.05 level.

Results

SNP heritability by all common autosomal SNPs

We first estimated the proportion of individual variability in DTI parameters of WM tracts that can be explained by the additive effects of all common autosomal SNPs. Figures 1-2 and Supplementary Figures 2-9 display the SNP heritability estimates of DTI parameters for the 21 main WM tracts. The associated standard errors, raw and FDR-adjusted p-values from the one-sided likelihood ratio tests are given in Supplementary Table 3. Genetic factors account for a moderate or large portion of the

variance of DTI parameters in almost all WM tracts. For example, genetic effects explained more than 60% of the total variance of FA in the posterior limb of the internal capsule (PLIC), anterior corona radiata (ACR), superior longitudinal fasciculus (SLF), cingulum cingulate gyrus (CGC), anterior limb of the internal capsule, and genu of the corpus callosum (GCC). SNP heritability of FA decreased to 28% and 22%, respectively, in the corticospinal tract (CST) and fornix (FX). The heritability in the last two tracts was consistently reported to be low across previous studies (Kochunov P *et al.* 2015). The 42 WM sub-tracts, most of which are left/right pairs, also show SNP heritability (Supplementary Table 3). Noticeable evidence of symmetry in SNP heritability was observed on the WM sub-tracts (Supplementary Figures 10-16).

The SNP heritability of FA, AD (L1), RD, MD, MO, L2 and L3 is similar to each other on almost all WM tracts. We also estimated sex-specific heritability of each DTI parameter on the 21 main WM tracts (Supplementary Figures 17-23), and found sex-specific modifications on SNP heritability for several WM tracts, but detected no systematic pattern across tracts by the two-sample t test (p-value = 0.419). The distribution of SNP

heritability was largely consistent across all, female, and male individuals. According to the functions of the main WM tracts (Connectopedia Knowledge Database, http://www.fmritools.com/kdb/white-matter/), we clustered them into four communities: complex fibers (C1), associative fibers (C2), commissural fibers (C3) and projection fibers (C4). We found that the set of WM tracts in C1 and C3 tended to have higher SNP heritability than those in C2 and C4.

Partitioning genetic variation by chromosome

To examine the distribution of SNP heritability across the genome, we partitioned SNP data into 22 chromosomes and fit the GRMs separately in 22 models. We found that the aggregated heritability across all of the 21 main WM tracts explained by each chromosome was linearly associated with the length of the chromosome (Figure 3(a), R^2 = 61.3%, p-value = $1.630*10^{-05}$). These findings reveal a highly polygenic or omnigenic genetic architecture (Boyle EA *et al.* 2017) of WM tracts. The large number of SNPs that contribute to the variation in DTI parameters are widely spread across the whole genome.

To further illustrate this architecture, we ordered and clustered the 22 chromosomes into three groups by their lengths: long, medium, and short. The long group had 4 chromosomes (CHRs 2, 1, 6, 3), which together accounted for 33% of the length of the whole genome; the medium group had 6 chromosomes (CHRs 4, 5, 7, 8, 10, 11), which accounted for another 33% of the length of the whole genome; and the short group consisted of the remaining 12 chromosomes. Figure 3(b) shows the SNP heritability grouped by chromosomal length for each of the seven DTI parameters. It is clear that longer chromosomes tended to have higher SNP heritability than shorter ones for all DTI parameters. We repeated the above two analyses with fitting the 22 GRMs simultaneously in one model, similar patterns are shown in Supplementary Figures 24(a) and (b).

Partitioning genetic variation by functional annotation

To compare the contribution of SNPs with different activity level, we partitioned the genetic variation according to CNS-cell-specific annotations: CNS_active, CNS_inactive,

and Always_inactive. Heritability estimated by SNPs residing in chromatin regions inactive across all cell groups (Always_inactive, mean heritability 1.3%) is significantly smaller than the heritability estimated by SNPs residing in chromatin regions active in CNS cell (CNS_active, mean heritability 2.5%, p-value < $2.210*10^{-16}$). The mean heritability estimated by CNS_inactive SNPs (inactive in CNS cell but active in other cells) is 2.0% (Supplementary Figure 24(c)). Since each category has different number of SNPs, it is difficult to compare the average contribution by one single SNP in different categories. To address this concern, we randomly selected the same number of SNPs from each SNP group and re-computed the heritability in each tract. We repeated the random selection 50 times. Again, we found that on average SNPs residing in CNS_active group (mean heritability 3.8%) contributed more to DTI heritability than other SNPs in Always_inactive group (mean heritability 2.0%) or CNS_inactive group (mean heritability 2.5%) (Figure 3(c)). This pattern remained consistent across all of the seven DTI parameters, though larger variance was observed for the MO parameter.

Genetic correlation across DTI parameters and WM tracts

In bivariate analyses, we show the genetic correlation map of DTI parameters and WM tracts. We verified that both FA and RD had positive genetic correlation with AD (L1) on most of the WM tracts, while FA and RD had strong negative correlation on all of the main WM tracts (Supplementary Table 4, Supplementary Figure 25). Similarly, L1 had positive genetic correlation with L2 and L3 on many of the main WM tracts, and L2 and L3 had strong positive correlation on all of the main WM tracts (Supplementary Table 4, Supplementary Figure 26). We also displayed the significant linear association (p-value < $2.661*10^{-05}$) between genetic correlations and the corresponding phenotypic correlations across WM tracts, which indicates that the estimated genetic correlations are robustly proportional to the phenotypic correlations across WM tracts.

The genetic correlation on pairs of the main WM tracts for each DTI parameter are displayed in Figure 4, Supplementary Table 5-11 and Supplementary Figure 27. For MD and RD, substantive genetic correlation was detected on many pairs of WM tracts; for AD (L1) and FA, the genetic correlations were generally smaller compared to those of MD or AD and more concentrated on pairs within C1 and C3. In particular, the three

corpus callosum tracts, the body of the corpus callosum (BCC), splenium of the corpus callosum (SCC), and GCC, showed consistently strong genetic correlations for each DTI parameter, except MO, which had few significant genetic correlations, representing a pattern that was distinct from those of the other DTI parameters.

Voxel-level analysis on TBSS skeleton

We selected several highly heritable tracts to conduct voxel-wise analysis on the TBSS skeleton, including GCC (p = 1834), ACR (p = 3129), superior corona radiata (SCR, p = 2778), SLF (p = 3503) and PLIC (p = 1775). We first compared the empirical density of the tract-mean and voxel-wise values of different DTI parameters on the GCC tract across subjects (Supplementary Figure 28), and found that the tract-mean and voxel-wise values of MO have quite different density shapes. Supplementary Figures 29-36 display the voxel-wise SNP heritability estimates on the selected TBSS skeleton. For each DTI parameter, the voxel-wise SNP heritability estimates are smaller than their tract-based estimates. In particular, MO showed small SNP heritability estimates on GCC, ACR, SCR, and SLF, which may be due to its non-Gaussian distribution of voxel-wise data. However,

for the other DTI parameters, some findings from the voxel-based analysis were indeed consistent with those from the tract-based analysis. Voxel-based analysis also indicated that the selected tracts are heritable for FA, AD (L1), RD, MD, L2 and L3 (Supplementary Figures 37-38). In addition, heritability of DTI parameters had significant linear relationship on some WM tracts, such as those for FA and RD on GCC, SLF, and PLIC (Supplementary Figures 39-40).

Shared genetic basis with neuropsychiatric traits

We examined the genetics overlap between DTI parameters and neuropsychiatric disorders using polygenic risk scores (Consortium IS 2009; Dudbridge F 2013; Hagenaars SP et al. 2016; Pasaniuc B and AL Price 2017). With FDR controlled at 0.05 level, we found 29 significant associations out of 588 tests: 18 for ADHD, 8 for ASD, 2 for SCZ, and one for BD (Figure 5). The estimated associations, standard errors, raw p-values and the R^2 of significant disorder-DTI pairs are given in Supplementary Table 4 (R^2 range [0.095%, 0.197%], mean R^2 0.120%, p-value range [$7.880*10^{-05}$, $3.851*10^{-03}$])**.** Genetics risk of ADHD was significantly associated with DTI parameters for several WM tracts include

PLIC, ALIC, RLIC, ACR, and PCR (R^2 range [0.097%, 0.197%], p-value range [$7.880*10^{-05}$, $3.851*10^{-03}$]). Most of the detected associations are negative. Higher polygenic risk of ASD was positively associated with L2, L3, MR and RD parameters for GCC (R^2 range [0.095%, 0.113%], p-value range [$9.973*10^{-04}$, $2.783*10^{-03}$]) and CGC (R^2 range [0.099%, 0.117%], p-value range [$1.420*10^{-03}$, $2.684*10^{-03}$]). For SCZ and BD, we found three significant associations with L1 for BCC and inferior fronto-occipital fasciculus (IFO).

Discussion

Uncovering the genetic architecture usually serves as the initial step in imaging genetics, providing the rationale for downstream analyses to model the causal genes and pathways involved in the phenotype of interest. A large number of family-based neuroimaging studies have documented that WM tracts are essentially heritable across the lifespan. However, the landscape of genetic contributions to DTI parameters of WM microstructures remains largely unknown. Here, our application in the UK Biobank dataset revealed the power of using common autosomal SNPs to understand the genetic basis of WM tracts. Our global heritability estimates are close to the ones

reported in previous family-based studies (Table 1 of Vuoksimaa E *et al.* (2017)). A recent GWAS of brain imaging phenotypes released by UK Biobank also reported that many diffusion MRI measures are heritable (Table 1 of Elliott LT et al. (2018)). Although the DTI parameters are generated using different pipelines, our tract-based heritability estimates are within a similar range as those reported in Elliott LT *et al.* (2018) (mean heritability around 45%). This verified that most of the WM tracts in UK Biobank are significantly heritable, regardless of which DTI parameter was used. We further illustrate that the voxel-wise DTI parameters show lower heritability than their tract-based counterpart. These results also suggest that studies of DTI phenotypes using common SNPs may be more informative than studies focused on rare variants. More importantly, our results partitioning the genetic variation in chromosomes or SNP functional sets shed light on the distribution of genetic signals across the genome and different functional consequences. As the UK Biobank releases more imaging data, it can be expected that future genetic analysis on heritable WM tracts will facilitate gene exploration, diseases/disorders risk prediction and heterogeneity dissection on WM microstructures.

The bivariate analysis of several pairs of DTI parameters shows that the genetic correlation of two DTI parameters (such as L2 and L3) is highly associated with their phenotypic correlation across WM tracts, after adjusting for the effects of fixed covariates. That is, a large proportion of the similarity of two DTI parameters can be consistently explained by their genetic similarity (R^2 > 60% for all pairs), which may reflect the non-specificity of the diffusion parameters and these DTI parameters consistently share very similar genetic bases across WM tracts. Perhaps for more biologically relevant tissue parameters, such as free water, axon diameters, and disambiguated anisotropies, genetic similarity would be less high. The genetic correlation analysis for pairs of WM tracts confirms a genetic link among WM tracts, especially for the set of complex or commissural fibers, such as corpus callosum tracts BCC, GCC and SCC.

We find significant genetic overlap for ADHD and multiple DTI parameters spanning several WM tracts, particularly for internal capsule tracts PLIC, RLIC, and ALIC. Previous

study (Elliott LT *et al.* 2018) found strong genetic correlation between ADHD and BCC and SLF tracts with using the LD score regression methods (Bulik-Sullivan BK *et al.* 2015). We also find genetic overlap for ASD and multiple DTI parameters of cingulum cingulate gyrus and corpus callosum. The phenotypic association between ASD and cingulum and corpus callosum has been consistently reported (Travers BG et al. 2012; Ismail MM et al. 2016; Aoki Y et al. 2017). Since the DTI parameters are also heritable, the substantial level of shared genetic variation indicates the power of using brain WM structure changes to predict mental health status in imaging genetics. However, due to the relatively small sample size, the variation in DTI parameters that can be explained by significant polygenic risks are all less than 0.2%. Currently, less than 1% R^2 is often reported in similar cross-traits studies for highly heritable neuropsychiatric disorders (Power RA et al. 2015; Clarke T et al. 2016; Socrates A et al. 2017; Bogdan R et al. 2018; Mistry S et al. 2018).

Our heritability analyses reflect several other methodological limitations of the current approaches on population-based imaging genetic studies. First, similar to previous

studies (Kochunov P *et al.* 2015), CST and FX were reported to have low SNP heritability, which may be due to the fact that such small, tubular tracts cannot be well registered and reliably resolved with current techniques (Bach M et al. 2014). Second, heritability estimated by SNP data reflects narrow-sense heritability, which only considers the additive genetic effects of common variants. The genetic architecture may change as we broadly consider all genetic contributions (such as rare variants, non-additive effects and gene-gene interactions) in future studies. However, it is notable that with common SNPs in the UK Biobank, we have gained heritability estimates comparable to those reported in family-based studies. In addition, the LMM-based approaches used in SNP heritability estimation requires a relatively large sample size. Previous studies show that the standard error of heritability estimates typically scales with 316/N, where N is the sample size (Visscher PM et al. 2014; Ge T et al. 2015). However, current imaging genetics studies usually have small sample size. When we estimate SNP heritability in the PING and PNC datasets with less than 1000 samples, few significant findings were found (Supplementary Figures 41-42). We also run simple simulations to illustrate the noisy SNP heritability estimates for small sample size (Supplementary Figure 43). Our

tract-based and voxel-based analyses on the MO parameter also indicate that the LMM-based SNP heritability estimation may be sensitive to the distribution of the phenotypes. LMMs may have poor performance on non-Gaussian distributed phenotypes such as MO voxel values. Finally, it is worth mentioning that the UK Biobank data are sampled from a specific cohort (British ancestry) with a specific age-range. Since genetic ancestries are common confounding effects and aging can play an important role in brain WM structure changes, one should be careful to generalize these findings to general populations or to specific clinical cohorts. With more data from population-based imaging genetics studies, future research will be required to overcome these limitations and improve our biological understanding of the human brain.

Funding

This work was supported by the National Institutes of Health (MH086633, MH092335 and MH116527), the National Science Foundation (SES-1357666 and DMS-1407655), a

grant from the Cancer Prevention Research Institute of Texas, and the endowed Bao-Shan Jing Professorship in Diagnostic Imaging.

Acknowledgements

We thank the individuals represented in the UK Biobank, PING and PNC datasets for their participation and the research teams for their work in collecting, processing and disseminating these datasets for analysis. This research has been conducted using the UK Biobank resource (application number 22783), subject to a data transfer agreement. Part of the data collection and sharing for this project was funded by the Pediatric Imaging, Neurocognition and Genetics Study (PING) (U.S. National Institutes of Health Grant RC2DA029475). PING is funded by the National Institute on Drug Abuse and the Eunice Kennedy Shriver National Institute of Child Health & Human Development. PING data are disseminated by the PING Coordinating Center at the Center for Human Development, University of California, San Diego. Support for the collection of the PNC datasets was provided by grant RC2MH089983 awarded to Raquel Gur and RC2MH089924 awarded to Hakon Hakonarson. All PNC subjects were recruited through

the Center for Applied Genomics at The Children's Hospital in Philadelphia. The authors acknowledge the Texas Advanced Computing Center (TACC, http: //www.tacc.utexas.edu) at The University of Texas at Austin for providing HPC and storage resources that have contributed to the research results reported within this paper.

Conflict of interest

The authors declare no competing financial interests.

REFERENCES

Alfaro-Almagro F, Jenkinson M, Bangerter NK, Andersson JL, Griffanti L, Douaud G, Sotiropoulos S, Jbabdi S, Fernandez MH, Vallee E. 2017. Image Processing and Quality Control for the first 10,000 Brain Imaging Datasets from UK Biobank. bioRxiv:130385.

Aoki Y, Yoncheva YN, Chen B, Nath T, Sharp D, Lazar M, Velasco P, Milham MP, Di Martino A. 2017. Association of white matter structure with autism spectrum disorder and attention-deficit/hyperactivity disorder. JAMA psychiatry 74:1120-1128.

Bach M, Laun FB, Leemans A, Tax CM, Biessels GJ, Stieltjes B, Maier-Hein KH. 2014. Methodological considerations on tract-based spatial statistics (TBSS). Neuroimage 100:358-369.

Badano JL, Katsanis N. 2002. Beyond Mendel: an evolving view of human genetic disease transmission. Nature reviews Genetics 3:779.

Basser PJ, Mattiello J, LeBihan D. 1994. Estimation of the effective self-diffusion tensor from the NMR spin echo. Journal of Magnetic Resonance, Series B 103:247-254.
Beaulieu C. 2002. The basis of anisotropic water diffusion in the nervous system–a technical review. NMR in Biomedicine 15:435-455.
Bogdan R, Baranger DA, Agrawal A. 2018. Polygenic risk scores in clinical psychology: bridging genomic risk to individual differences. Annual review of clinical psychology 14:119-157.
Boyle EA, Li YI, Pritchard JK. 2017. An Expanded View of Complex Traits: From Polygenic to Omnigenic. Cell 169:1177-1186.
Brouwer RM, Mandl RC, Peper JS, van Baal GCM, Kahn RS, Boomsma DI, Pol HEH. 2010. Heritability of DTI and MTR in nine-year-old children. Neuroimage 53:1085-1092.
Brouwer RM, Mandl RC, Schnack HG, van Soelen IL, van Baal GC, Peper JS, Kahn RS, Boomsma DI, Pol HH. 2012. White matter development in early puberty: a longitudinal volumetric and diffusion tensor imaging twin study. PloS one 7:e32316.
Bulik-Sullivan BK, Loh P-R, Finucane HK, Ripke S, Yang J, Patterson N, Daly MJ, Price AL, Neale BM, Consortium SWGotPG. 2015. LD Score regression distinguishes confounding from polygenicity in genome-wide association studies. Nature genetics 47:291-295.
Chiang M-C, Barysheva M, Toga AW, Medland SE, Hansell NK, James MR, McMahon KL, De Zubicaray GI, Martin NG, Wright MJ. 2011. BDNF gene effects on brain circuitry replicated in 455 twins. Neuroimage 55:448-454.
Clarke T, Lupton M, Fernandez-Pujals A, Starr J, Davies G, Cox S, Pattie A, Liewald D, Hall L, MacIntyre D. 2016. Common polygenic risk for autism spectrum disorder (ASD) is associated with cognitive ability in the general population. Molecular psychiatry 21:419.
Consortium IS. 2009. Common polygenic variation contributes to risk of schizophrenia and bipolar disorder. Nature 460:748.
Cox SR, Ritchie SJ, Tucker-Drob EM, Liewald DC, Hagenaars SP, Davies G, Wardlaw JM, Gale CR, Bastin ME, Deary IJ. 2016. Ageing and brain white matter structure in 3,513 UK Biobank participants. Nature communications 7:13629.
Davis LK, Yu D, Keenan CL, Gamazon ER, Konkashbaev AI, Derks EM, Neale BM, Yang J, Lee SH, Evans P. 2013. Partitioning the heritability of Tourette syndrome and obsessive compulsive disorder reveals differences in genetic architecture. PLoS genetics 9:e1003864.

Demontis D, Walters RK, Martin J, Mattheisen M, Als TD, Agerbo E, Belliveau R, Bybjerg-Grauholm J, Bækved-Hansen M, Cerrato F. 2017. Discovery of the first genome-wide significant risk loci for ADHD. BioRxiv:145581.
Dudbridge F. 2013. Power and predictive accuracy of polygenic risk scores. PLoS genetics 9:e1003348.
Elliott LT, Sharp K, Alfaro-Almagro F, Shi S, Miller KL, Douaud G, Marchini J, Smith SM. 2018. Genome-wide association studies of brain imaging phenotypes in UK Biobank. Nature 562:210.
Finucane HK, Bulik-Sullivan B, Gusev A, Trynka G, Reshef Y, Loh P-R, Anttila V, Xu H, Zang C, Farh K. 2015. Partitioning heritability by functional annotation using genome-wide association summary statistics. Nature genetics 47:1228-1235.
Ge T, Nichols TE, Lee PH, Holmes AJ, Roffman JL, Buckner RL, Sabuncu MR, Smoller JW. 2015. Massively expedited genome-wide heritability analysis (MEGHA). Proceedings of the National Academy of Sciences 112:2479-2484.
Geng X, Gouttard S, Sharma A, Gu H, Styner M, Lin W, Gerig G, Gilmore JH. 2012. Quantitative tract-based white matter development from birth to age 2years. Neuroimage 61:542-557.
Hagenaars SP, Harris SE, Davies G, Hill WD, Liewald DC, Ritchie SJ, Marioni RE, Fawns-Ritchie C, Cullen B, Malik R. 2016. Shared genetic aetiology between cognitive functions and physical and mental health in UK Biobank (N= 112 151) and 24 GWAS consortia. Molecular psychiatry 21:1624.
Ismail MM, Keynton RS, Mostapha MM, ElTanboly AH, Casanova MF, Gimel'farb GL, El-Baz A. 2016. Studying autism spectrum disorder with structural and diffusion magnetic resonance imaging: a survey. Frontiers in human neuroscience 10:211.
Jenkinson M, Beckmann CF, Behrens TE, Woolrich MW, Smith SM. 2012. Fsl. Neuroimage 62:782-790.
Jernigan TL, Brown TT, Hagler DJ, Akshoomoff N, Bartsch H, Newman E, Thompson WK, Bloss CS, Murray SS, Schork N. 2016. The pediatric imaging, neurocognition, and genetics (PING) data repository. Neuroimage 124:1149-1154.
Jones DK, Knösche TR, Turner R. 2013. White matter integrity, fiber count, and other fallacies: the do's and don'ts of diffusion MRI. Neuroimage 73:239-254.

Kanchibhotla SC, Mather KA, Wen W, Schofield PR, Kwok JB, Sachdev PS. 2013. Genetics of ageing-related changes in brain white matter integrity–A review. Ageing research reviews 12:391-401.
Kochunov P, Jahanshad N, Marcus D, Winkler A, Sprooten E, Nichols TE, Wright SN, Hong LE, Patel B, Behrens T. 2015. Heritability of fractional anisotropy in human white matter: a comparison of Human Connectome Project and ENIGMA-DTI data. Neuroimage 111:300-311.
Lee SH, DeCandia TR, Ripke S, Yang J, Sullivan PF, Goddard ME, Keller MC, Visscher PM, Wray NR, Consortium SPG-WAS. 2012. Estimating the proportion of variation in susceptibility to schizophrenia captured by common SNPs. Nature genetics 44:247-250.
Lee SH, Ripke S, Neale BM, Faraone SV, Purcell SM, Perlis RH, Mowry BJ, Thapar A, Goddard ME, Witte JS. 2013. Genetic relationship between five psychiatric disorders estimated from genome-wide SNPs. Nature genetics 45:984.
Lee SJ, Steiner RJ, Luo S, Neale MC, Styner M, Zhu H, Gilmore JH. 2015. Quantitative tract-based white matter heritability in twin neonates. NeuroImage 111:123-135.
Lee SJ, Steiner RJ, Yu Y, Short SJ, Neale MC, Styner MA, Zhu H, Gilmore JH. 2017. Common and heritable components of white matter microstructure predict cognitive function at 1 and 2 y. Proceedings of the National Academy of Sciences 114:148-153.
Loh P-R, Bhatia G, Gusev A, Finucane HK, Bulik-Sullivan BK, Pollack SJ, de Candia TR, Lee SH, Wray NR, Kendler KS. 2015. Contrasting genetic architectures of schizophrenia and other complex diseases using fast variance-components analysis. Nature genetics 47:1385-1392.
Mistry S, Harrison JR, Smith DJ, Escott-Price V, Zammit S. 2018. The use of polygenic risk scores to identify phenotypes associated with genetic risk of bipolar disorder and depression: A systematic review. Journal of affective disorders.
Nir TM, Jahanshad N, Villalon-Reina JE, Toga AW, Jack CR, Weiner MW, Thompson PM, Initiative AsDN. 2013. Effectiveness of regional DTI measures in distinguishing Alzheimer's disease, MCI, and normal aging. NeuroImage: clinical 3:180-195.
Pasaniuc B, Price AL. 2017. Dissecting the genetics of complex traits using summary association statistics. Nature Reviews Genetics 18:117.

Penke L, Maniega SM, Bastin M, Hernández MV, Murray C, Royle N, Starr J, Wardlaw J, Deary I. 2012. Brain-wide white matter tract integrity is associated with information processing speed and general intelligence. Molecular psychiatry 17:955.
Penke L, Maniega SM, Murray C, Gow AJ, Hernández MCV, Clayden JD, Starr JM, Wardlaw JM, Bastin ME, Deary IJ. 2010. A general factor of brain white matter integrity predicts information processing speed in healthy older people. Journal of Neuroscience 30:7569-7574.
Power RA, Steinberg S, Bjornsdottir G, Rietveld CA, Abdellaoui A, Nivard MM, Johannesson M, Galesloot TE, Hottenga JJ, Willemsen G. 2015. Polygenic risk scores for schizophrenia and bipolar disorder predict creativity. Nature neuroscience 18:953.
Purcell S, Neale B, Todd-Brown K, Thomas L, Ferreira MA, Bender D, Maller J, Sklar P, De Bakker PI, Daly MJ. 2007. PLINK: a tool set for whole-genome association and population-based linkage analyses. The American Journal of Human Genetics 81:559-575.
Ritchie SJ, Bastin ME, Tucker-Drob EM, Maniega SM, Engelhardt LE, Cox SR, Royle NA, Gow AJ, Corley J, Pattie A. 2015. Coupled changes in brain white matter microstructure and fluid intelligence in later life. Journal of Neuroscience 35:8672-8682.
Ritchie SJ, Booth T, Hernández MdCV, Corley J, Maniega SM, Gow AJ, Royle NA, Pattie A, Karama S, Starr JM. 2015. Beyond a bigger brain: Multivariable structural brain imaging and intelligence. Intelligence 51:47-56.
Ruderfer DM, Ripke S, McQuillin A, Boocock J, Stahl EA, Pavlides JMW, Mullins N, Charney AW, Ori AP, Loohuis LMO. 2018. Genomic Dissection of Bipolar Disorder and Schizophrenia, Including 28 Subphenotypes. Cell 173:1705-1715. e1716.
Satterthwaite TD, Elliott MA, Ruparel K, Loughead J, Prabhakaran K, Calkins ME, Hopson R, Jackson C, Keefe J, Riley M. 2014. Neuroimaging of the Philadelphia neurodevelopmental cohort. Neuroimage 86:544-553.
Sklar P. 2017. Psychiatric Genomics Consortium: Past And Present. European Neuropsychopharmacology 27:S359.
Smith SM, Jenkinson M, Johansen-Berg H, Rueckert D, Nichols TE, Mackay CE, Watkins KE, Ciccarelli O, Cader MZ, Matthews PM. 2006. Tract-based spatial statistics: voxelwise analysis of multi-subject diffusion data. Neuroimage 31:1487-1505.

Socrates A, Bond T, Karhunen V, Auvinen J, Rietveld C, Veijola J, Jarvelin M-R, O'Reilly P. 2017. Polygenic risk scores applied to a single cohort reveal pleiotropy among hundreds of human phenotypes. bioRxiv:203257.
Storey JD. 2002. A direct approach to false discovery rates. Journal of the Royal Statistical Society: Series B (Statistical Methodology) 64:479-498.
Sudlow C, Gallacher J, Allen N, Beral V, Burton P, Danesh J, Downey P, Elliott P, Green J, Landray M. 2015. UK biobank: an open access resource for identifying the causes of a wide range of complex diseases of middle and old age. PLoS medicine 12:e1001779.
Sudre G, Choudhuri S, Szekely E, Bonner T, Goduni E, Sharp W, Shaw P. 2017. Estimating the Heritability of Structural and Functional Brain Connectivity in Families Affected by Attention-Deficit/Hyperactivity Disorder. JAMA psychiatry 74:76-84.
Sullivan PF, Agrawal A, Bulik CM, Andreassen OA, Børglum AD, Breen G, Cichon S, Edenberg HJ, Faraone SV, Gelernter J. 2017. Psychiatric genomics: an update and an agenda. American Journal of Psychiatry 175:15-27.
Tamnes CK, Østby Y, Walhovd KB, Westlye LT, Due-Tønnessen P, Fjell AM. 2010. Intellectual abilities and white matter microstructure in development: a diffusion tensor imaging study. Human brain mapping 31:1609-1625.
Tamnes CK, Roalf DR, Goddings A-L, Lebel C. 2017. Diffusion MRI of white matter microstructure development in childhood and adolescence: methods, challenges and progress. Developmental cognitive neuroscience.
Thomason ME, Thompson PM. 2011. Diffusion imaging, white matter, and psychopathology. Annual review of clinical psychology 7.
Thompson PM, Stein JL, Medland SE, Hibar DP, Vasquez AA, Renteria ME, Toro R, Jahanshad N, Schumann G, Franke B. 2014. The ENIGMA Consortium: large-scale collaborative analyses of neuroimaging and genetic data. Brain imaging and behavior 8:153-182.
Timpson NJ, Greenwood CM, Soranzo N, Lawson DJ, Richards JB. 2017. Genetic architecture: the shape of the genetic contribution to human traits and disease. Nature Reviews Genetics.
Travers BG, Adluru N, Ennis C, Tromp DP, Destiche D, Doran S, Bigler ED, Lange N, Lainhart JE, Alexander AL. 2012. Diffusion tensor imaging in autism spectrum disorder: a review. Autism Research 5:289-313.

Visscher PM, Hemani G, Vinkhuyzen AA, Chen G-B, Lee SH, Wray NR, Goddard ME, Yang J. 2014. Statistical power to detect genetic (co) variance of complex traits using SNP data in unrelated samples. PLoS genetics 10:e1004269.
Vogel K, Timmers I, Kumar V, Nickl-Jockschat T, Bastiani M, Roebroek A, Herpertz-Dahlmann B, Konrad K, Goebel R, Seitz J. 2016. White matter microstructural changes in adolescent anorexia nervosa including an exploratory longitudinal study. NeuroImage: Clinical 11:614-621.
Voineskos AN. 2015. Genetic underpinnings of white matter 'connectivity': heritability, risk, and heterogeneity in schizophrenia. Schizophrenia research 161:50-60.
Vuoksimaa E, Panizzon MS, Hagler Jr DJ, Hatton SN, Fennema-Notestine C, Rinker D, Eyler LT, Franz CE, Lyons MJ, Neale MC. 2017. Heritability of white matter microstructure in late middle age: A twin study of tract-based fractional anisotropy and absolute diffusivity indices. Human brain mapping 38:2026-2036.
Yang J, Benyamin B, McEvoy BP, Gordon S, Henders AK, Nyholt DR, Madden PA, Heath AC, Martin NG, Montgomery GW. 2010. Common SNPs explain a large proportion of the heritability for human height. Nature genetics 42:565.
Yang J, Lee SH, Goddard ME, Visscher PM. 2011. GCTA: a tool for genome-wide complex trait analysis. The American Journal of Human Genetics 88:76-82.
Yang J, Manolio TA, Pasquale LR, Boerwinkle E, Caporaso N, Cunningham JM, De Andrade M, Feenstra B, Feingold E, Hayes MG. 2011. Genome partitioning of genetic variation for complex traits using common SNPs. Nature genetics 43:519.
Zhao B, Zou F. 2018. Is Polygenic Risk Scores Prediction Good? bioRxiv:447797.

Captions to figures

Figure 1. SNP heritability of 21 main WM tracts grouped by tract functions from the UK Biobank dataset.

Figure 2. SNP heritability of 21 main WM tracts from the UK Biobank dataset.

Figure 3. SNP heritability of 21 main WM tracts by chromosome or SNP categories from the UK Biobank dataset.

Figure 4. Genetic correlation in pairs of main WM tracts grouped by tract functions.

Figure 5. Associations between the polygenic profiles of seven psychiatric disorders created from the published GWAS summary statistics, and 21 main WM tracts in the UK Biobank dataset.

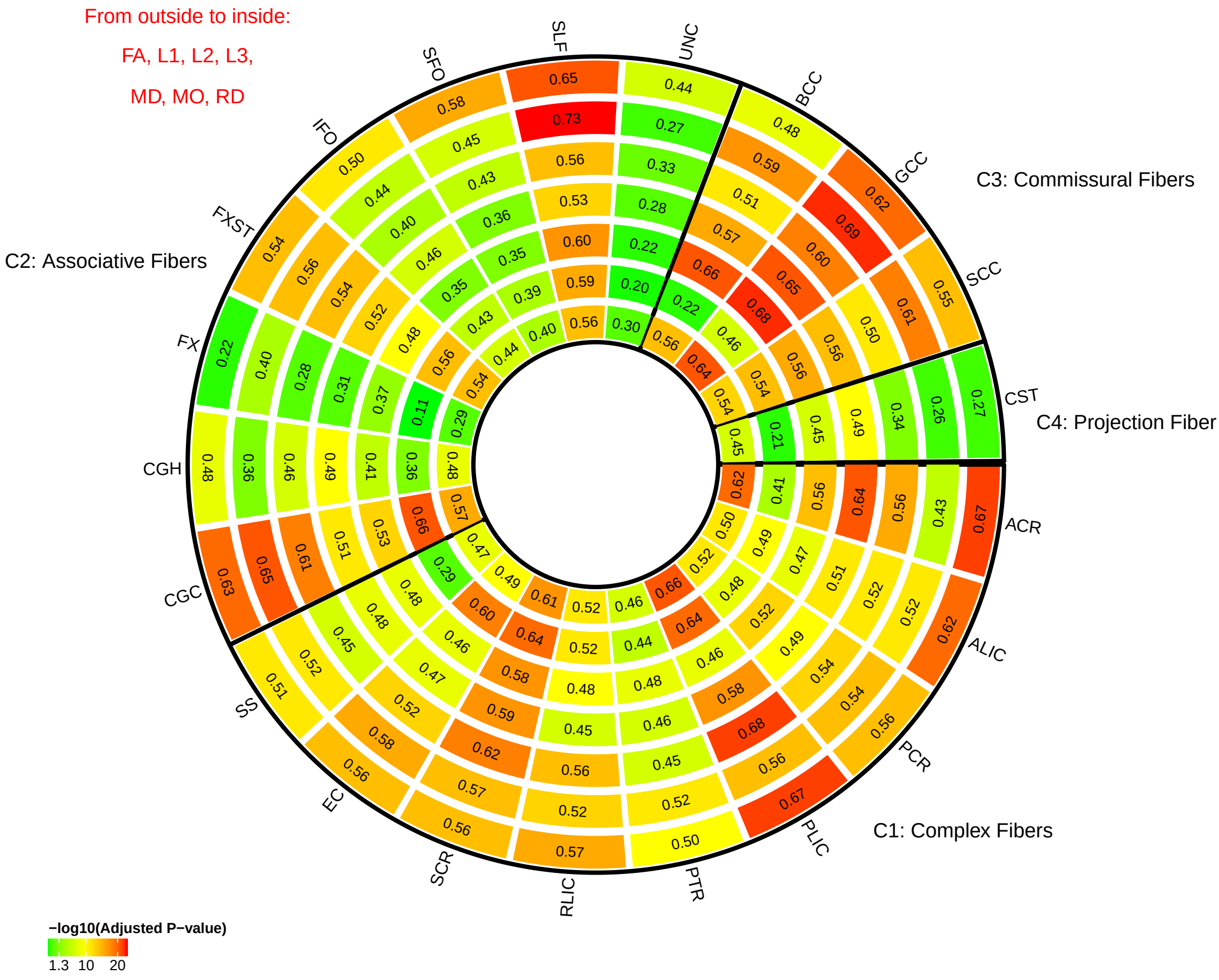
From outside to inside:
FA, L1, L2, L3,
MD, MO, RD
C2: Associative Fibers
C3: Commissural Fibers
C4: Projection Fiber
C1: Complex Fibers
FX
CGH
CGC
SS
EC
SCR
RLIC
PTR
PLIC
PCR
ALIC
ACR
CST
SCC
GCC
BCC
UNC
SLF
SFO
IFO
FXST
−log10(Adjusted P−value)
1.3
10
20

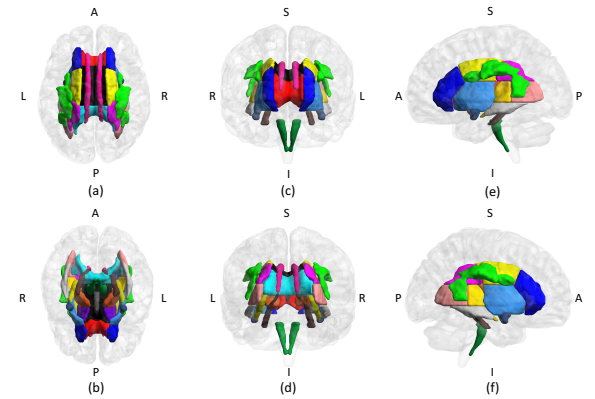

(a) Superior view (b) Inferior view (c) Anterior view (d) Posterior view (e) Left view (f) Right view

(a) WM Main Tracts Annotation

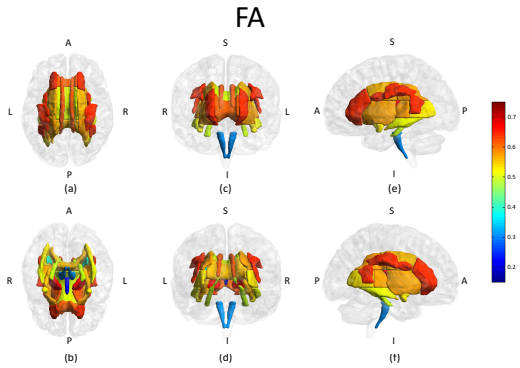

(a) Superior view (b) Inferior view (c) Anterior view (d) Posterior view (e) Left view (f) Right view

(b)

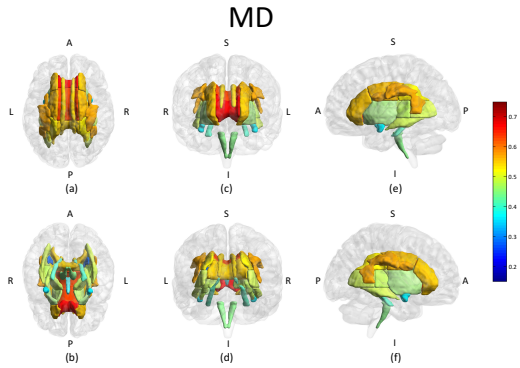

(a) Superior view (b) Inferior view (c) Anterior view (d) Posterior view (e) Left view (f) Right view

(c)

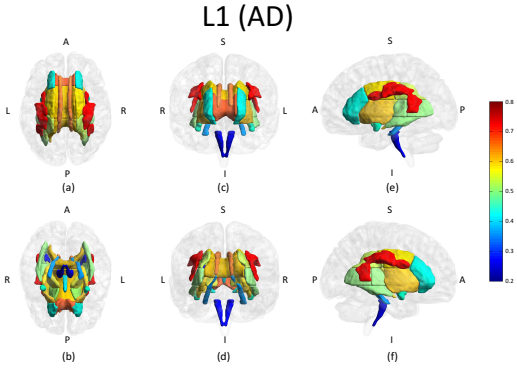

(a) Superior view (b) Inferior view (c) Anterior view (d) Posterior view (e) Left view (f) Right view

(d)

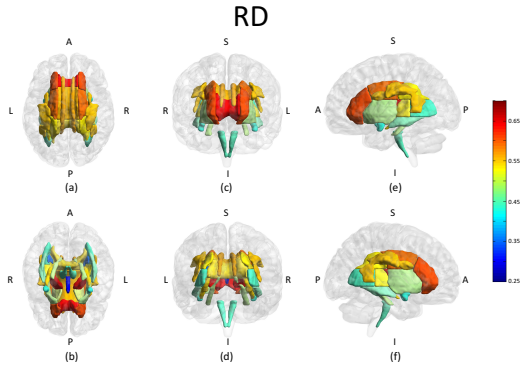

(a) Superior view (b) Inferior view (c) Anterior view (d) Posterior view (e) Left view (f) Right view

(e)

A

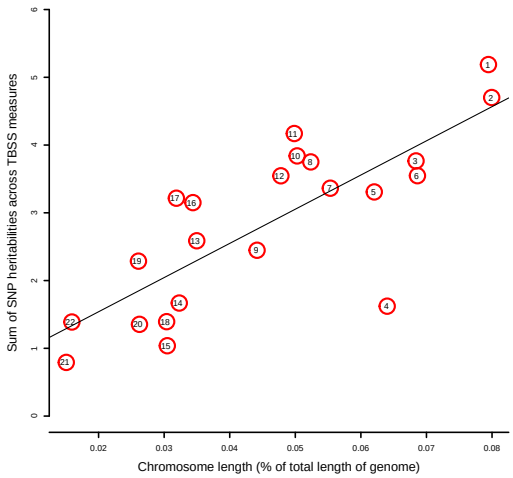

(a) Aggregated SNP heritability of each chromosome.

B

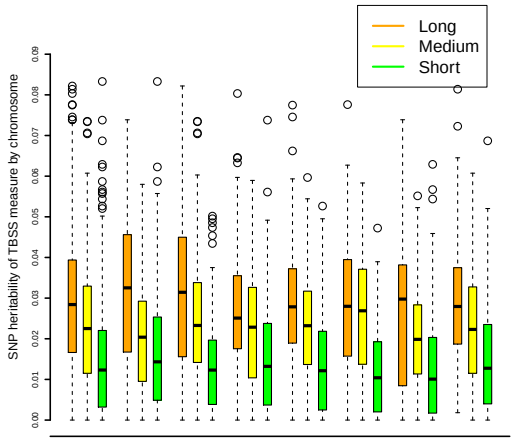

(b) SNP heritability grouped by chromosome length.

C

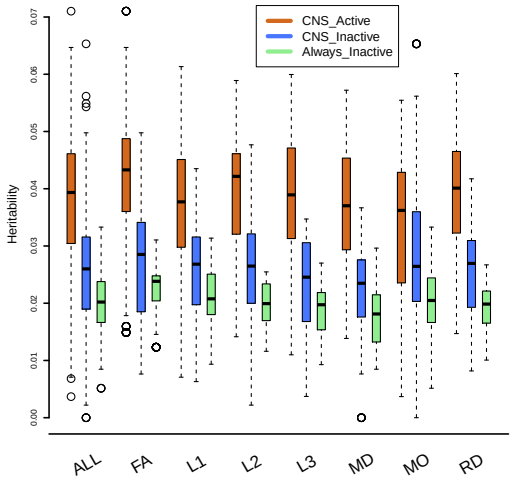

(c) SNP heritability grouped by CNS functional annotations.

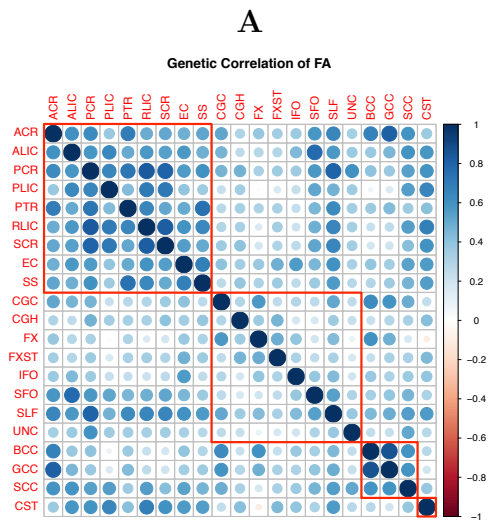

(a) FA

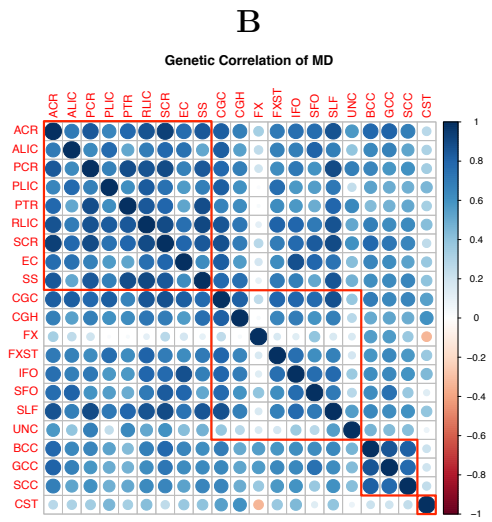

(b) MD

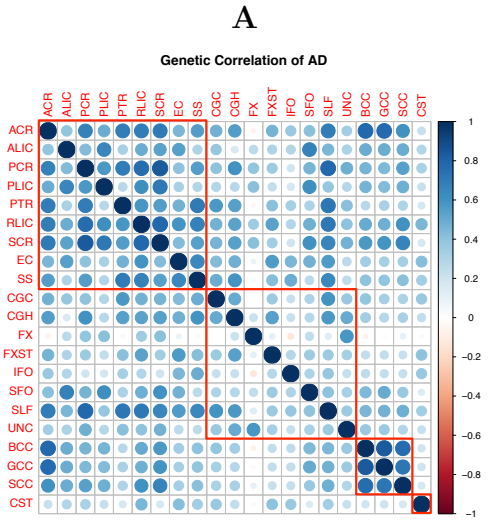

(c) L1 (AD)

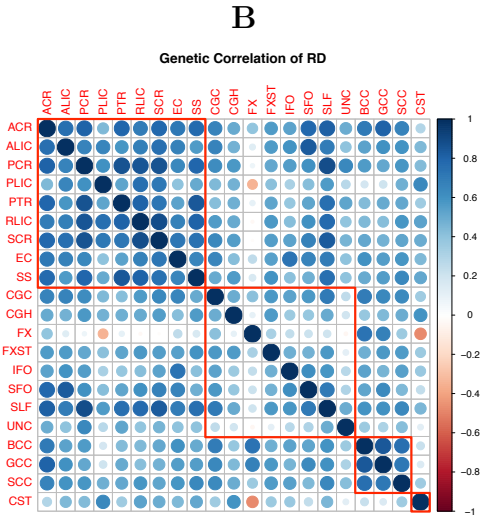

(d) RD

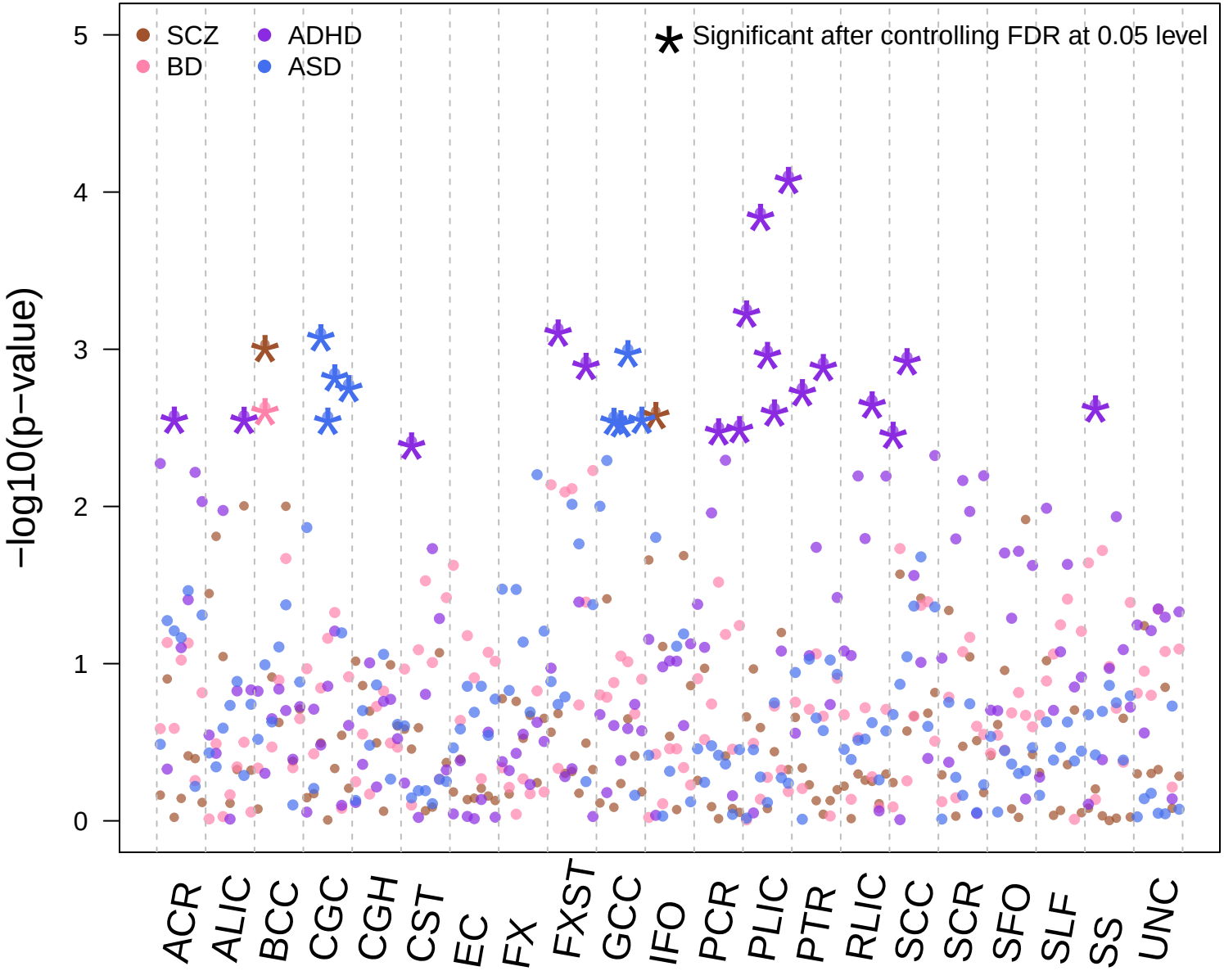
SCZ
BD
ADHD
ASD
Significant after controlling FDR at 0.05 level
−log10(p−value)
0
1
2
3
4
5
ACR
ALIC
BCC
CGC
CGH
CST
EC
FX
FXST
GCC
IFO
PCR
PLIC
PTR
RLIC
SCC
SCR
SFO
SLF
SS
UNC